Proceedings of CONF-MSS 2026 Syposium: Mechanical Control and Automation
DOI: 10.54254/2755-2721/2026.BJ32494

CFD Analysis of Adjustable Rear Wing Effects on Aerodynamic Performance of F1 Race Car

Yilin Wu

St. Croix Lutheran Academy, West St. Paul, USA
ianwu6369@gmail.com

Abstract. The aim of this study is to examine the aerodynamic characteristics of a 2018 Formula 1 car rear wing, which is equipped with a Drag Reduction System (DRS), by applying a two-dimensional computational fluid dynamics (CFD) approach, particularly when the DRS is partially activated. The study applied a commercial CFD code, ANSYS Fluent, based on a k-omega Shear Stress Transport (SST) turbulence closure model, to solve the flow problem. The CFD code was applied to a 2018 Formula 1 car rear wing to solve the aerodynamic problem for different DRS activation ratios, i.e., 0%, 25%, 50%, 75%, and 100%, at three different free-stream velocities, i.e., 50 m/s, 70 m/s, and 90 m/s. The results obtained in this study indicated that although aerodynamic forces are proportional to the square of the free-stream velocity, lift and drag coefficients remain almost constant for a wide range of free-stream velocities. The results reveal a "sweet spot" where a 25% opening of the DRS resulted in a 50% reduction in drag and a 20-22% increase in downforce compared to a fully closed DRS position due to a "slot effect" delaying the flow separation. The results obtained in this study revealed that the highest opening of the DRS, i.e., 100% DRS, resulted in a 75% reduction in drag but caused a significant reduction in downforce.

Keywords: CFD, Drag Reduction System, Aerodynamic Optimization, Multi-element Airfoil

1. Introduction

In Formula 1, the rear wing is one of the critical components in achieving an aerodynamic compromise [1]. The rear wing needs to produce sufficient downforce in order to achieve stability during high-speed cornering, while at the same time reducing drag in order to prevent a corresponding loss in car speed on the straights. This requirement has led to the development of increasingly sophisticated rear wing designs, particularly in the era of multi-element devices. The Drag Reduction System (DRS) represents the most direct approach in achieving an aerodynamic compromise [2]. The DRS reduces aerodynamic drag by moving the upper flap of the rear wing, allowing faster speeds on the straights. However, the DRS is typically viewed as a binary system, either fully closed or fully open, in both technical discussions and aerodynamic analysis. This assumption, however, represents a limitation in the analysis, as the DRS system is not considered in terms of a range of different states. This paper explores whether there is a linear relationship between aerodynamic performance and changes in tail flap angle between the closed and open DRS

© 2026 The Authors. This is an open access article distributed under the terms of the Creative Commons Attribution License 4.0 (https://creativecommons.org/licenses/by/4.0/).

DOI: 10.54254/2755-2721/2026.BJ32494

configurations, and thus determines a possible, better drag-downforce ratio. Thus, a CFD study was performed on a tail flap geometry that complies with the 2018 regulations.

2. Materials and methods

2.1. Model description

This research is intended to investigate the aerodynamic performance of the Formula 1 rear wing with the DRS system, based on the high downforce rear wing design that is applicable to the 2018 Formula 1 Regulation Period, specifically the Scuderia Ferrari SF71H specification [3]. The period was a transition in the development of the aerodynamics of the Formula 1 car, where the multi-element rear wing still had high levels of geometrical complexity, and the DRS system was an essential component in the development of the aerodynamics of the Formula 1 car. The design provides an excellent balance and represents the aerodynamic trade-off in the generation of downforce and drag reduction well. However, in order to achieve high-quality 3D simulations, the flow should be solved in three-dimensional space, resulting in a tremendous increase in the cost and unnecessary complexity of the simulation process. In order to overcome the limitations of the simulation process, the physics-based dimensional reduction strategy was adopted in the simulation process, specifically in the aerodynamic performance aspects. The center plane airfoil was manually isolated from the 3D CAD design. The high-resolution point coordinates were adopted in the main plane and the flap, specifically 201 coordinate points in the main plane and the flap. The profiles were able to maintain the original curve and the thickness distribution of the original 3D design at high levels of precision. The scaling was carried out by determining the ray length from the standard reference point of the design. The chord lengths of the main plane and the flap were determined to be 271.47 mm and 130.55 mm, which were then used to determine the open angle and the coordinates of the openness of the flap on the rear wing.

This study modeled the actuation of DRS as a rigid-body rotation about a pivot point, which is representative of the real-world Formula 1 mechanical actuation. The pivot point was defined as (x, y) = (439.97, 270.41). The flap was then rotated through five discrete configurations from closed (0°, baseline), 25% open (7.84°), 50% open (15.68°), 75% open (23.53°), to fully open (31.37°). This range of flap rotation corresponds to a range of vertical displacements from 21 mm (the minimum gap as defined by the regulations) to 85 mm (fully open). This naturally varies the gap between the main plane and the flap as the flap is rotated, ensuring the effects of aerodynamic interaction are naturally modeled.

2.2. Simulation setup

All the aerodynamic simulations were carried out using the ANSYS Fluent software, following a structured approach to ensure the guidelines set by CFD research are adhered to [4]. The computational domain was created around the two-dimensional airfoil assembly in the form of a C-shape, which minimizes the effects of artificial accelerations. The inlet was set as a semi-circular inlet boundary, 15 meters upstream from the leading edge, allowing the flow to develop fully before reaching the airfoil. The outlet was set 15 meters beyond the leading edge, allowing the wake to develop fully. Simulations were carried out for three different freestream velocities, typical of those found in F1 racing: 50 m/s (approximately 180 km/h) for medium-speed cornering, 70 m/s (approximately 252 km/h) for high-speed cornering, and 90 m/s (approximately 324 km/h). A grid independence analysis was performed, confirming the suitability of the baseline mesh, which had

DOI: 10.54254/2755-2721/2026.BJ32494

approximately 26,000 to 27,000 quadrilateral elements, as the aerodynamic coefficients were the same for both the baseline and the finer meshes. The fluid was assumed to be an incompressible, Newtonian fluid with constant properties, simulating the conditions found in the atmosphere. The study was conducted at a speed lower than Mach 0.3, thus allowing the study to neglect the effects of compressibility. Reference values were established, where the unit reference area was taken as 1 m^2, and the unit reference span, which is the depth, was taken as 1 m. This was because the study was two-dimensional. The lift and drag coefficients were calculated, and the lift coefficient was negative, indicating the generation of downforce. The boundary and initial conditions were established, where the flow was considered to be uniform and constant. The upstream boundary condition was considered to be a pressure inlet, thus enabling the flow to develop stably towards the airfoil. This also reduced the numerical sensitivity to the location of the inlet. The downstream boundary condition was considered to be a pressure outlet, where the pressure was set to 0 Pa, which is the atmospheric pressure. This ensured the flow was convected smoothly through the domain and no artificial pressure reflections were felt at the downstream boundary. The flow was considered to be turbulent, and the parameters were set to a 5 percent intensity and a viscosity ratio of 10.

2.3. Computational method

A manually controlled, structured refinement strategy was employed. The final computational grid had approximately 26,000 to 27,000 quadrilateral grid elements, depending on the particular value of the DRS angle. This method enabled the mesh density to be increased in the aerodynamically critical areas, yet the total number of grid cells to remain within reasonable limits. The computational domain was meshed using geometric partition lines, which aid in the refinement process. A refinement region was set to a value at x=0.15m, as this is the region of the highest flow acceleration and the highest level of suction. The region is critical and requires the highest level of mesh density to correctly resolve the rapid pressure gradients and to avoid oscillations. A second vertical partition line was set on the trailing edge, where $x \approx 0.44$ m. A dedicated wake region was created downstream of the plane. The boundary layer, composed of prismatic elements, was meshed along all airfoil surfaces, aligned in the direction of the flow. The mesh enabled the velocities and the airflow to be analyzed, and the particular phenomena were particularly pronounced in the vicinity of the flaps as the DRS angle increased.

All simulations employed the k–ω Shear Stress Transport (SST) turbulence model. Convergence of the solutions was monitored using both numerical and physical criteria [5]. Convergence of all residuals was set to a value of 1e-6 [6]. Lift coefficient (C_L) and drag coefficient (C_D) monitors were also monitored during the simulation process. For each condition, up to 10,000 iterations were performed. Only after the stabilization of these values over a few hundred iterations was the convergence complete. This double validation of convergence ensured that the trends observed in downforce loss and drag reduction were not due to numerical artifacts but reflected actual aerodynamic behavior. The turbulent intensity was set to a value of 5%, and the turbulent viscosity ratio was set to a value of 10. This is a moderate level of freestream turbulence and is a common value used for external aerodynamic simulations. The same values were also applied to the backflow conditions at the outlet. Uniform freestream conditions were used to start the simulation process as per the given conditions of the inlet velocity. This model integrates the benefits of the standard k-ω formulation near solid walls and the k-ε model behavior in the free-stream region. This model is applicable for flows with strong adverse pressure gradients and separation. The equation for the turbulent kinetic energy k is given by:

DOI: 10.54254/2755-2721/2026.BJ32494

$$\frac{\partial(\rho k)}{\partial t} + \frac{\partial}{\partial x_j}(\rho u_j k) = \frac{\partial}{\partial x_j}\left[\left(\mu + \frac{\mu_t}{\sigma_k}\right)\frac{\partial k}{\partial x_j}\right] + P_k - \rho \tag{1}$$

$$\frac{\partial(\rho\omega)}{\partial t} + \frac{\partial(\rho u_j \omega)}{\partial x_j} = \alpha\frac{\rho\omega}{k}P_k - \beta\rho\omega^2 + \frac{\partial}{\partial x_j}\left[\left(\mu + \frac{\mu_t}{\sigma_\omega}\right)\frac{\partial \omega}{\partial x_j}\right] + 2(1-F_1)\rho\sigma_{\omega 2}\frac{1}{\omega}\frac{\partial k}{\partial x_j}\frac{\partial \omega}{\partial x_j} \tag{2}$$

In these equations, P_K represents the generated turbulent kinetic energy and μ_t is the turbulent viscosity [7]. The ability of the model to predict fluid separation and reattachment is improved by setting an upper limit on the turbulent shear stress in the SST equations. This property makes the k-ω SST model applicable to multi-element airfoils, where the interaction between the high-pressure gradient and the wake can be observed, as well as to wake structures with a partially open DRS. The artificial wake is generated by integrating airfoil pressure and viscous shear stresses. The obtained forces are decomposed into lift and drag according to the direction of the freestream velocity. Therefore, the lift and drag coefficients C_L and C_D are defined as follows:

$$C_L = \frac{L}{\frac{1}{2}\rho U_\infty^2 S} \tag{3}$$

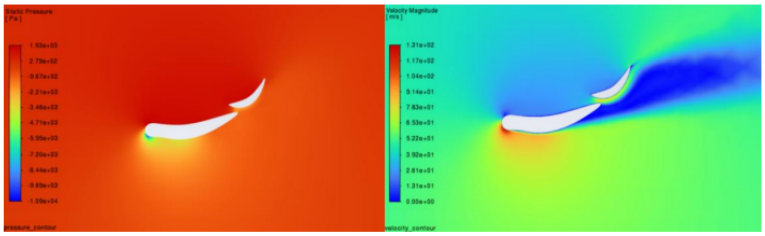
$$C_D = \frac{D}{\frac{1}{2}\rho U_\infty^2 S} \tag{4}$$

where L is the total lift, D is the total drag, ρ is the air density, and U_∞ is the free stream velocity. The reference area S is derived from the unit span and unit reference length, consistent with the two-dimensional modeling framework used in this study; a value of $C_L \leq 0$ produces a downforce, which is the rule for the aerodynamic notation used in the analysis of this study.

3. Results and discussion

3.1. Wind speed effects

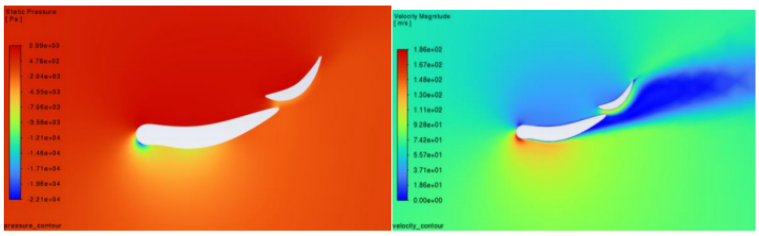
Simulations were performed at freestream velocities of 50 m/s, 70 m/s, and 90 m/s, as depicted in Figures 1–15. The lift and drag coefficients were nearly constant. In the case of the baseline configuration with 0% DRS, the drag coefficient reduced slightly from 0.093 to 0.089, and the lift coefficient changed from -0.78 to -0.81.



(a) (b)

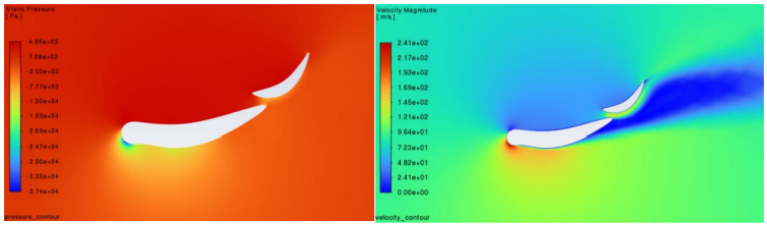
Figure 1. (a) Static pressure (b) Velocity magnitude DRS = 0%, U_∞ = 50m/s

DOI: 10.54254/2755-2721/2026.BJ32494



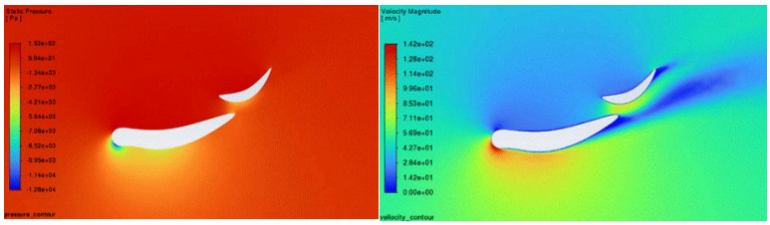
(a) (b)

Figure 2. (a) Static pressure (b) Velocity magnitude DRS = 0%, U_{∞} = 70m/s



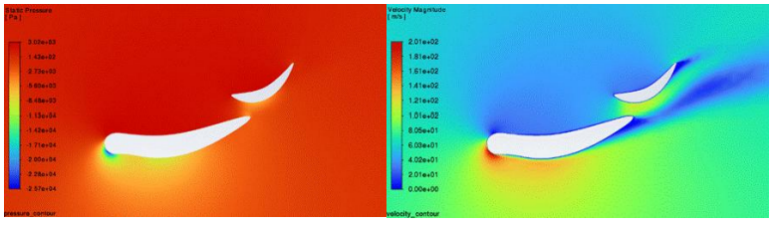
(a) (b)

Figure 3. (a) Static pressure (b) Velocity magnitude DRS = 0%, U_{∞} = 90m/s



(a) (b)

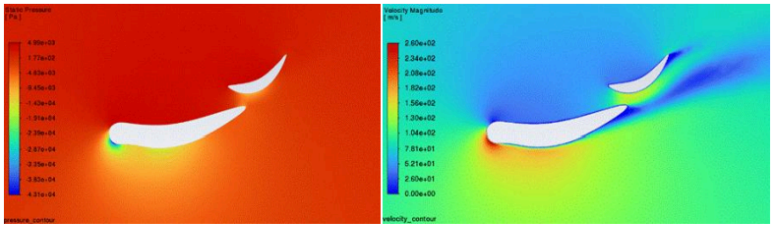
Figure 4. (a) Static pressure (b) Velocity magnitude DRS = 25%, U∞ = 50m/s



(a) (b)

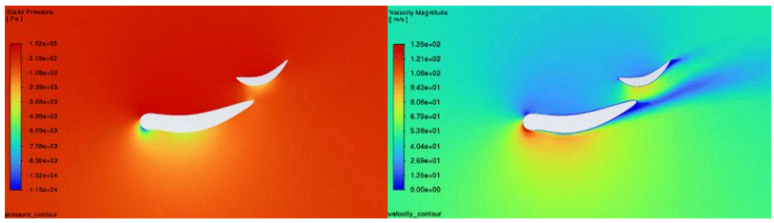
Figure 5. (a) Static pressure (b) Velocity magnitude DRS = 25%, U_{∞} = 70m/s

DOI: 10.54254/2755-2721/2026.BJ32494



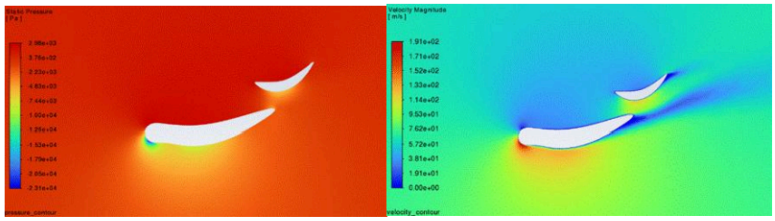
(a) (b)

Figure 6. (a) Static pressure (b) Velocity magnitude DRS = 25%, U_∞ = 90m/s



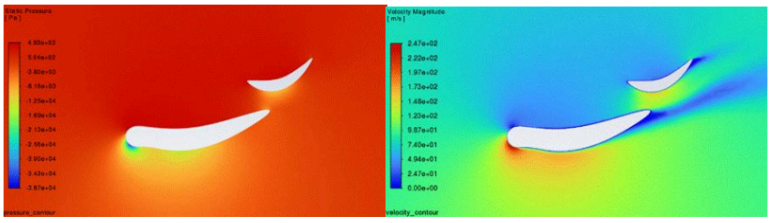
(a) (b)

Figure 7. (a) Static pressure (b) Velocity magnitude DRS = 50%, U_∞ = 50m/s



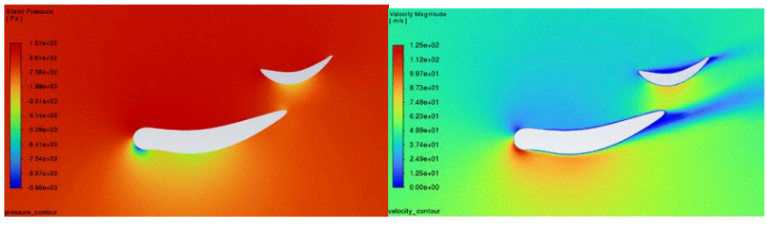
(a) (b)

Figure 8. (a) Static pressure (b) Velocity magnitude DRS = 50%, U_∞ = 70m/s



(a) (b)

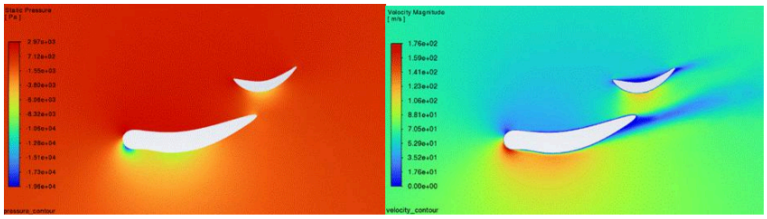
Figure 9. (a) Static pressure (b) Velocity magnitude DRS = 50%, U_∞ = 90m/s



(a) (b)

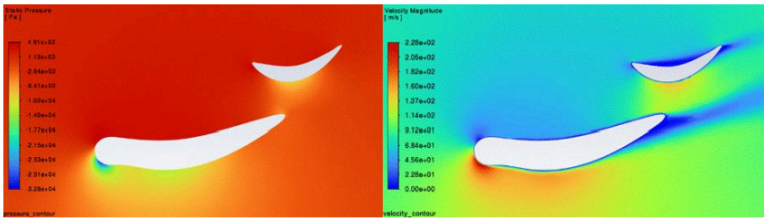
Figure 10. (a) Static pressure (b) Velocity magnitude DRS = 75%, U_∞ = 50m/s

DOI: 10.54254/2755-2721/2026.BJ32494



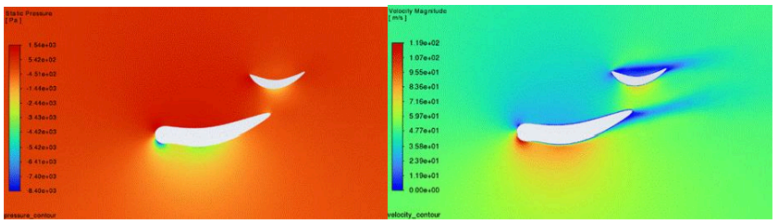
(a) (b)

Figure 11. (a) Static pressure (b) Velocity magnitude DRS = 75%, U_∞ = 70m/s



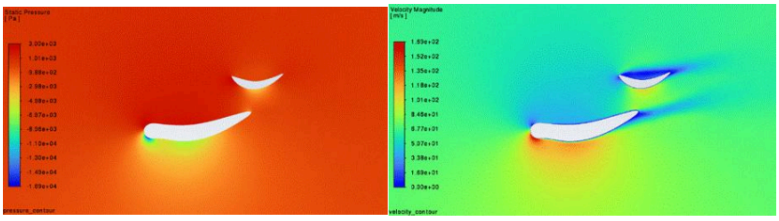
(a) (b)

Figure 12. (a) Static pressure (b) Velocity magnitude DRS = 75%, U_∞ = 90m/s



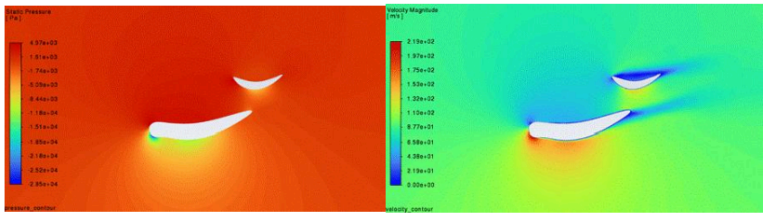
(a) (b)

Figure 13. (a) Static pressure (b) Velocity magnitude DRS = 100%, U_∞ = 50m/s



(a) (b)

Figure 14. (a) Static pressure (b) Velocity magnitude DRS = 100%, U_∞ = 70m/s



(a) (b)

Figure 15. (a) Static pressure (b) Velocity magnitude DRS = 100%, U_∞ = 90m/s

DOI: 10.54254/2755-2721/2026.BJ32494

3.2. Impact of rear wing adjustments

A nonlinear response to the changes in the aerodynamics was observed. For small DRS opening, the gap between the main plane and the flap acts as an aerodynamic slot, which allows the high-energy flow from the pressure side of the main plane to re-energize the suction side of the flap. This slot effect can delay the flow separation and increase the pressure recovery [8]. In some instances, the downforce can be increased, and the pressure drag can be reduced. This effect diminishes as the opening of the DRS increases. The camber of the wing is reduced, the suction peak on the flap is reduced, and the wake becomes larger due to increased flow detachment. The reduction of the drag is dominated by the geometrical unloading, and the downforce is reduced. This nonlinear effect shows the possibility of the flap opening providing the best compromise between drag reduction and downforce retention. This nonlinear effect can be used to develop more refined DRS control strategies. Another significant observation was the fact that, with a freestream velocity of 50 m/s, the drag coefficient, as illustrated in Figure 16(A), reduced from 0.0935 in the fully closed state to 0.0490 at 25% DRS opening, which was a reduction of nearly 50% using only a quarter of the available DRS opening range. As the DRS opening was increased, the rate of drag reduction was reduced, reaching 0.0241 at 100% opening. This also indicates that the major contributor to drag in the fully closed state is the large-scale separation effects and the associated low-pressure wake created by the DRS flap itself [8].

The simulations also indicated that the maximum downforce was obtained when the DRS was set to 25% opening, as illustrated in Figure 16(B). At 90 m/s, the lift coefficient increased in magnitude from -0.813 to -0.996 as the opening was increased from 0% to 25%. As the opening was increased further, the lift coefficient was reduced dramatically, reaching -0.634 at 100% opening. Thus, the effect is geometry driven, indicating the effects are not velocity dependent. Thus, the optimum range is for intermediate opening, but 100% opening is the best state for the long straight sections where terminal velocity is the priority, and downforce is of less consequence.

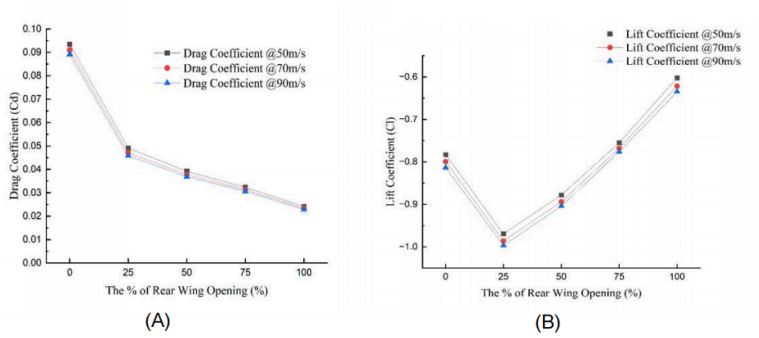


Figure 16. (A) The drag coefficient result (B) The lift coefficient result

4. Conclusion

The focus of this study is to analyze the aerodynamic behavior of DRS tail flaps using 2D CFD simulations, specifically the effect of partial DRS opening on the tail design of a Formula 1 car. The analysis was performed for different DRS flap opening positions and free-flow velocities, as well as in combination with the general high-downforce tail design of 2018. The analysis shows that the lift and drag coefficients do not vary significantly with free-stream velocity over the velocity range tested. Furthermore, this behavior supports the fact that the dimensionless aerodynamic coefficient serves as a reasonable performance comparison tool for rear wings under different operating

DOI: 10.54254/2755-2721/2026.BJ32494

conditions. In particular, the results show that the DRS opens and the aerodynamic behavior is strongly nonlinear. Rather than a simple switch between high downforce and low drag states, the trailing wing behavior shows a clear aerodynamic sweet spot in both low and partial DRS states. Compared to the fully closed state, opening the flaps by about 25% increases downforce while drag is disproportionately reduced. As the DRS flaps are opened further, the effect of the flaps on the aerodynamic behavior gradually decreases. The decrease in drag is accompanied by a decrease in the drag reduction rate, and when the transition to a fully low drag state occurs, downforce is significantly reduced. This behavior suggests an important design insight, namely that the DRS does not need to be fully open to achieve optimal aerodynamic efficiency, but can be partially activated to achieve a reasonable balance between drag reduction and downforce.

References

[1] Katz, J. (2006). Race car aerodynamics: Designing for speed (2nd ed.). Bentley Publishers.
[2] Newey, A. (2017). How to build a car. HarperCollins.
[3] Fédération Internationale de l'Automobile. (2018, March 9). 2018 Formula One technical regulations (Issue 3). https: //www.fia.com/regulation/category/110
[4] ANSYS, Inc. (2025). Ansys Fluent theory guide. https: //ansyshelp.ansys.com/public/Views/Secured/corp/v251/en/pdf/Ansys_Fluent_Theory_Guide.pdf
[5] Menter, F. R. (1994). Two-equation eddy-viscosity turbulence models for engineering applications. AIAA Journal, 32(8), 1598–1605. https: //doi.org/10.2514/3.12149
[6] Versteeg, H. K., & Malalasekera, W. (2007). An introduction to computational fluid dynamics: The finite volume method (2nd ed.). Pearson Education.
[7] Wilcox, D. C. (2006). Turbulence modeling for CFD (3rd ed.). DCW Industries.
[8] Schlichting, H., & Gersten, K. (2016). Boundary-layer theory (9th ed.). Springer. https: //doi.org/10.1007/978-3-662-52919-5